Total- and Scattered-Field Decomposition Technique for the Finite-Element Time-Domain Modeling of Buried Scatterers

Zheng Lou, *Student Member, IEEE*, L. E. Rickard Petersson, *Member, IEEE*, Jian-Ming Jin, *Fellow, IEEE*, and Douglas J. Riley

***Abstract*—The total- and scattered-field decomposition (TSFD) technique, developed earlier for scattering in free space, is extended for the finite-element time-domain (FETD) modeling of scattering by an object either residing above, partially embedded, or completely buried in a lossy dielectric half-space. The formulation leads to both a volumetric and a Huygens' surface method to excite an incident field in the total-field region. Numerical examples demonstrate the accuracy and the flexibility of the method.**

***Index Terms*—Buried objects, field decomposition, finite-element method, time-domain analysis.**

I. Introduction

THE finite-element time-domain (FETD) method has recently been recognized as a promising computational technique for electromagnetic simulation because of its excellent geometrical modeling capability and its ability to perform broadband characterization and to model nonlinear inhomogeneous media. For open-region scattering problems, the FETD method is traditionally formulated in terms of either the total or the scattered field [1]. The scattered-field formulation is usually preferred because it eliminates the dispersion error in the total-field formulation associated with the propagation of the incident field from the boundary of the computational domain (absorbing boundary) to the scatterer. However, for certain applications where the scattered field nearly cancels the incident field so that the resulting total field is rather small, it is more desirable to work with the total field to obtain a more accurate solution. In such a case, a better approach is to split the computational domain into an interior total-field region (which tightly encloses the scatterer) and an exterior scattered-field region. One such approach was reported in [2], where two schemes were described to effectively excite the incident field in the total-field region. In particular, it was shown that a volumetric excitation scheme was capable of exciting a perfect incident field with zero leakage into the scattered-field region.

Manuscript received January 28, 2005; revised February 15, 2005. This work was supported in part by the Department of Defense's High Performance Computing Modernization Program under Contract HPTi-PET-2001-024 and in part by the Air Force Office of Scientific Research via the MURI Program under Contract FA9550-04-1-0326.

Z. Lou, L. E. Rickard Petersson, and J.-M. Jin are with the Department of Electrical and Computer Engineering, University of Illinois at Urbana–Champaign, Urbana, IL 61801-2991 USA.

D. J. Riley is with the Northrop Grumman Corporation, Albuquerque, NM 87109 USA.

Digital Object Identifier 10.1109/LAWP.2005.846158

In this paper, the total- and scattered-field decomposition (TSFD) technique, as developed in [2] for scattering in free space, is extended for the FETD modeling of scattering by an object either residing above, partially embedded, or completely buried in a lossy dielectric half-space. This is an important extension because a large number of electromagnetic problems fall into the category of determining the electromagnetic field scattered by objects in the presence of a dielectric half-space. Applications include buried target detection using ground-penetrating radars and nondestructive testing. This type of problems has traditionally been dealt with using the finite-difference time-domain (FDTD) method [3]–[5]. However, the FETD offers an attractive alternative. Different from the free-space case, the presence of the half-space medium requires the knowledge of not only the incident field but also the reflected and the transmitted fields from the air–dielectric interface. Since the loss of the half-space medium is considered frequency dispersive, both the reflected and the transmitted fields are computed in the frequency domain and converted into the time domain via a standard fast Fourier transform (FFT). As in [2], two TSFD formulations are presented here. One excites the incident/reflected/transmitted field (henceforth referred to as the impressed field) through the interface between the total- and scattered-field regions, and the other excites the impressed field through the volume of the total-field region. The accuracy of both formulations is investigated, and it is shown that the second approach once again provides a perfect excitation of the impressed field with zero leakage into the scattered-field region.

II. Formulation

The problem of interest is electromagnetic scattering from a scatterer (characterized by permeability μ, permittivity ε, and conductivity σ), which is either placed above, partially buried, or entirely buried in a homogeneous half-space medium, as shown in Fig. 1. The use of an absorbing boundary condition, such as a perfectly matched layer (PML), enables the truncation of the computation domain V with an outer boundary Ω_s. The proposed method splits the entire computation domain into an interior region V_t, where the field is represented by the total field, and an exterior region V_s, where the field is represented by the scattered field. The total-field region contains the entire

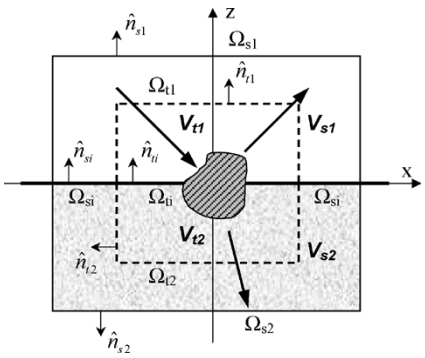

Fig. 1. Cross section of the total-field/scattered-field solution spaces with the lower half of the space filled with a homogeneous medium.

scatterer and is separated from the scattered-field region by the artificial boundary Ω_t. The presence of the air–dielectric interface further divides the two regions into four volumetric regions: V_{t1}, V_{t2}, V_{s1}, and V_{s2}, where the subscripts "1" and "2" stand for the regions above and below the air–dielectric interface, respectively. Except for the regions occupied by the scatterer, free space is assumed everywhere in the upper regions, whereas the lower regions are occupied by a lossy medium with permittivity ε_b and conductivity σ_b (the permeability of the medium is assumed to be the same as that of free space). In V_{t1} and V_{t2}, the second-order wave equation can be written with respect to the total field as

$$\nabla \times \left(\frac{1}{\mu}\nabla \times \mathbf{E}^t\right) + \varepsilon\frac{\partial^2}{\partial t^2}\mathbf{E}^t + \sigma\frac{\partial}{\partial t}\mathbf{E}^t = 0, \quad \text{for } V_{t1} \ \& \ V_{t2}. \tag{1}$$

Similarly, the wave equations for the scattered field are given by

$$\nabla \times \left(\frac{1}{\mu_0}\nabla \times \mathbf{E}^s\right) + \varepsilon_0\frac{\partial^2}{\partial t^2}\mathbf{E}^s = 0, \quad \text{for } V_{s1} \tag{2}$$

and

$$\nabla \times \left(\frac{1}{\mu_0}\nabla \times \mathbf{E}^s\right) + \varepsilon_b\frac{\partial^2}{\partial t^2}\mathbf{E}^s + \sigma_b\frac{\partial}{\partial t}\mathbf{E}^s = 0, \quad \text{for } V_{s2}. \tag{3}$$

On the truncation boundary Ω_s, one may use a PML or a boundary integral equation [1]. In this paper, for the sake of brevity, we simply use the first-order absorbing boundary condition (ABC)

$$\hat{n}_s \times \left(\frac{1}{\mu_0}\nabla \times \mathbf{E}^s\right) + Y\,\hat{n}_s \times \left(\hat{n}_s \times \frac{\partial}{\partial t}\mathbf{E}^s\right) = 0, \quad \text{on } \Omega_{s1} \ \& \ \Omega_{s2} \tag{4}$$

where Y is the intrinsic impedance of the medium ($Y = Y_0$ in the upper half-space and $Y = Y_b$ in the lower half-space medium).

A. Surface Excitation

Testing (1)–(4) with function $\mathbf{w}$ and invoking the divergence theorem, we can derive the weak forms of the above wave equations as given by

$$\begin{aligned}\iiint_{V_{t1}}\left\{\frac{1}{\mu}(\nabla\times\mathbf{w})\cdot\left(\nabla\times\mathbf{E}^t\right)+\varepsilon\,\mathbf{w}\cdot\frac{\partial^2}{\partial t^2}\mathbf{E}^t+\sigma\,\mathbf{w}\cdot\frac{\partial}{\partial t}\mathbf{E}^t\right\}dV \\ -\frac{1}{\mu_0}\iint_{\Omega_{t1}}(\hat{n}_{t1}\times\mathbf{w})\cdot\left(\nabla\times\mathbf{E}^t\right)d\Omega \\ +\iint_{\Omega_{ti}}\frac{1}{\mu}(\hat{n}_{ti}\times\mathbf{w})\cdot\left(\nabla\times\mathbf{E}^t\right)d\Omega=0\end{aligned} \tag{5}$$

for the total field in V_{t1}

$$\begin{aligned}\iiint_{V_{t2}}\left\{\frac{1}{\mu}(\nabla\times\mathbf{w})\cdot\left(\nabla\times\mathbf{E}^t\right)+\varepsilon\,\mathbf{w}\cdot\frac{\partial^2}{\partial t^2}\mathbf{E}^t+\sigma\,\mathbf{w}\cdot\frac{\partial}{\partial t}\mathbf{E}^t\right\}dV \\ -\frac{1}{\mu_0}\iint_{\Omega_{t2}}(\hat{n}_{t2}\times\mathbf{w})\cdot\left(\nabla\times\mathbf{E}^t\right)d\Omega \\ -\iint_{\Omega_{ti}}\frac{1}{\mu}(\hat{n}_{ti}\times\mathbf{w})\cdot\left(\nabla\times\mathbf{E}^t\right)d\Omega=0\end{aligned} \tag{6}$$

for the total field in V_{t2}

$$\begin{aligned}\iiint_{V_{s1}}\left\{\frac{1}{\mu_0}(\nabla\times\mathbf{w})\cdot(\nabla\times\mathbf{E}^s)+\varepsilon_0\,\mathbf{w}\cdot\frac{\partial^2}{\partial t^2}\mathbf{E}^s\right\}dV \\ +\frac{1}{\mu_0}\iint_{\Omega_{t1}}(\hat{n}_{t1}\times\mathbf{w})\cdot(\nabla\times\mathbf{E}^s)d\Omega \\ +\frac{1}{\mu_0}\iint_{\Omega_{si}}(\hat{n}_{si}\times\mathbf{w})\cdot(\nabla\times\mathbf{E}^s)d\Omega \\ +Y_0\iint_{\Omega_{s1}}(\hat{n}_{s1}\times\mathbf{w})\cdot\left(\hat{n}_{s1}\times\frac{\partial}{\partial t}\mathbf{E}^s\right)d\Omega=0\end{aligned} \tag{7}$$

for the scattered field in V_{s1}, and (8), shown at the bottom of the page, for the scattered field in V_{s2}. Combining (5)–(8) and denoting the impressed field as $\hat{\mathbf{E}}^i = \mathbf{E}^t - \mathbf{E}^s$, we obtain the weak-form wave equation for the entire system in (9), shown at the bottom of the next page. Note that in the above derivation, we assume the permeability to be μ_0 everywhere in the computational domain except for the region occupied by the scatterer. However, if the permeability is different across the air–dielectric

$$\begin{aligned}\iiint_{V_{s2}}\left\{\frac{1}{\mu_0}(\nabla\times\mathbf{w})\cdot(\nabla\times\mathbf{E}^s)+\varepsilon_b\mathbf{w}\cdot\frac{\partial^2}{\partial t^2}\mathbf{E}^s+\sigma_b\mathbf{w}\cdot\frac{\partial}{\partial t}\mathbf{E}^s\right\}dV \\ +\frac{1}{\mu_0}\iint_{\Omega_{t2}}(\hat{n}_{t2}\times\mathbf{w})\cdot(\nabla\times\mathbf{E}^s)d\Omega-\frac{1}{\mu_0}\iint_{\Omega_{si}}(\hat{n}_{si}\times\mathbf{w})\cdot(\nabla\times\mathbf{E}^s)d\Omega \\ +Y_b\iint_{\Omega_{s2}}(\hat{n}_{s2}\times\mathbf{w})\cdot\left(\hat{n}_{s2}\times\frac{\partial}{\partial t}\mathbf{E}^s\right)d\Omega=0\end{aligned} \tag{8}$$

interface, extra integral terms will appear in the equation above. By expanding all the various fields in terms of the same basis functions as the testing functions, (9) can be converted into the following matrix system:

$$\begin{bmatrix} \mathbf{T}^t & 0 \\ \mathbf{T}^{s,t} & \mathbf{T}^s \end{bmatrix} \begin{bmatrix} \frac{d^2}{dt^2}\boldsymbol{\alpha}^t \\ \frac{d^2}{dt^2}\boldsymbol{\alpha}^s \end{bmatrix} + \begin{bmatrix} \mathbf{B}^t & 0 \\ 0 & \mathbf{B}^s + \mathbf{P}^s \end{bmatrix} \cdot \begin{bmatrix} \frac{d}{dt}\boldsymbol{\alpha}^t \\ \frac{d}{dt}\boldsymbol{\alpha}^s \end{bmatrix} + \begin{bmatrix} \mathbf{S}^t & 0 \\ \mathbf{S}^{s,t} & \mathbf{S}^s \end{bmatrix} \begin{bmatrix} \boldsymbol{\alpha}^t \\ \boldsymbol{\alpha}^s \end{bmatrix} = \begin{bmatrix} 0 & 0 \\ \mathbf{T}^{s,t} & 0 \end{bmatrix} \begin{bmatrix} \frac{d^2}{dt^2}\tilde{\boldsymbol{\alpha}}^i \\ 0 \end{bmatrix} + \begin{bmatrix} \mathbf{Q}^t & 0 \\ \mathbf{S}^{s,t} & 0 \end{bmatrix} \begin{bmatrix} \tilde{\boldsymbol{\alpha}}^i \\ 0 \end{bmatrix} \quad (10)$$

where the expressions for the matrices in (10) can readily be inferred from (9), and $\boldsymbol{\alpha}^t$ and $\boldsymbol{\alpha}^s$ denote the unknowns associated with the total and scattered field, respectively. The unknowns residing on the boundary Ω_t can represent either the total or the scattered field and here we choose them to represent the total field, which yields $\mathbf{T}^{s,t}$ and $\mathbf{S}^{s,t}$ in the right-hand side of (10). As defined previously, $\tilde{\mathbf{E}}^i$ represents the difference between the total and the scattered fields. In the case of free-space scattering presented in [2], $\tilde{\mathbf{E}}^i$ is the same as the incident field $\mathbf{E}^i$. However, for the half-space scattering, $\tilde{\mathbf{E}}^i$ is the sum of the incident and the reflected fields above the air–dielectric interface, and it is the transmitted field below the interface. In both cases, $\tilde{\mathbf{E}}^i$ is a known analytical field and can be expanded in terms of basis functions in the same fashion as $\mathbf{E}^t$ and $\mathbf{E}^s$, and the corresponding projected coefficients are denoted by $\tilde{\boldsymbol{\alpha}}^i$. The hierarchical vector basis functions proposed by Webb [6] are used for the results presented in this paper, and the computation of the projected coefficients is described in [7]. There are various options available for discretizing (10) in time. For the results in this paper, we have employed the Newmark beta method that, when used properly, is unconditionally stable [1].

B. Volumetric Excitation

In the surface formulation described previously, the impressed field excitation is introduced to the system by a surface integral on the boundary Ω_t. In the following, we show that the impressed field excitation can be imposed in another fashion. By once again invoking the divergence theorem in the total-field region, we can easily prove the equality shown in (11) at the bottom of the page. Substituting (11) into (9) yields (12), shown at the bottom of the next page. Different from the surface excitation of the impressed field in (9), (12) represents an alternative formulation where the impressed field is applied as a volumetric source throughout the volume of the total-field region. The corresponding finite-element method (FEM) matrix equation of (12) is given by

$$\begin{bmatrix} \mathbf{T}^t & 0 \\ \mathbf{T}^{s,t} & \mathbf{T}^s \end{bmatrix} \begin{bmatrix} \frac{d^2}{dt^2}\boldsymbol{\alpha}^t \\ \frac{d^2}{dt^2}\boldsymbol{\alpha}^s \end{bmatrix} + \begin{bmatrix} \mathbf{B}^t & 0 \\ 0 & \mathbf{B}^s + \mathbf{P}^s \end{bmatrix} \cdot \begin{bmatrix} \frac{d}{dt}\boldsymbol{\alpha}^t \\ \frac{d}{dt}\boldsymbol{\alpha}^s \end{bmatrix} + \begin{bmatrix} \mathbf{S}^t & 0 \\ \mathbf{S}^{s,t} & \mathbf{S}^s \end{bmatrix} \begin{bmatrix} \boldsymbol{\alpha}^t \\ \boldsymbol{\alpha}^s \end{bmatrix} = \begin{bmatrix} \mathbf{T}^i & 0 \\ \mathbf{T}^{s,t} & 0 \end{bmatrix} \begin{bmatrix} \frac{d^2}{dt^2}\tilde{\boldsymbol{\alpha}}^i \\ 0 \end{bmatrix} + \begin{bmatrix} \mathbf{B}^i & 0 \\ 0 & 0 \end{bmatrix} \begin{bmatrix} \frac{d}{dt}\tilde{\boldsymbol{\alpha}}^i \\ 0 \end{bmatrix} + \begin{bmatrix} \mathbf{S}^i & 0 \\ \mathbf{S}^{s,t} & 0 \end{bmatrix} \begin{bmatrix} \tilde{\boldsymbol{\alpha}}^i \\ 0 \end{bmatrix} \quad (13)$$

where the expressions for all the matrices can be inferred from (12).

$$\begin{aligned} &\iiint_{V_t} \left\{ \frac{1}{\mu} (\nabla \times \mathbf{w}) \cdot (\nabla \times \mathbf{E}^t) + \varepsilon\, \mathbf{w} \cdot \frac{\partial^2}{\partial t^2}\mathbf{E}^s + \sigma\, \mathbf{w} \cdot \frac{\partial}{\partial t}\mathbf{E}^t \right\} dV \\ &\quad + \iiint_{V_{s1}} \left\{ \frac{1}{\mu_0} (\nabla \times \mathbf{w}) \cdot (\nabla \times \mathbf{E}^s) + \varepsilon_0\, \mathbf{w} \cdot \frac{\partial^2}{\partial t^2}\mathbf{E}^s \right\} dV \\ &\quad + \iiint_{V_{s2}} \left\{ \frac{1}{\mu_0} (\nabla \times \mathbf{w}) \cdot (\nabla \times \mathbf{E}^s) + \varepsilon_b\, \mathbf{w} \cdot \frac{\partial^2}{\partial t^2}\mathbf{E}^s + \sigma_b\, \mathbf{w} \cdot \frac{\partial}{\partial t}\mathbf{E}^s \right\} dV \\ &\quad + Y_0 \iint_{\Omega_{s1}} (\hat{n}_{s1} \times \mathbf{w}) \cdot \left(\hat{n}_{s1} \times \frac{\partial}{\partial t}\mathbf{E}^s \right) d\Omega + Y_b \iint_{\Omega_{s2}} (\hat{n}_{s2} \times \mathbf{w}) \cdot \left(\hat{n}_{s2} \times \frac{\partial}{\partial t}\mathbf{E}^s \right) d\Omega \\ &= \frac{1}{\mu_0} \iint_{\Omega_{t1}} (\hat{n}_{t1} \times \mathbf{w}) \cdot \left(\nabla \times \tilde{\mathbf{E}}^i \right) d\Omega + \frac{1}{\mu_0} \iint_{\Omega_{t2}} (\hat{n}_{t2} \times \mathbf{w}) \cdot \left(\nabla \times \tilde{\mathbf{E}}^i \right) d\Omega \end{aligned} \quad (9)$$

$$\begin{aligned} &\frac{1}{\mu_0} \iint_{\Omega_{t1}} (\hat{n}_{t1} \times \mathbf{w}) \cdot \left(\nabla \times \tilde{\mathbf{E}}^i \right) d\Omega + \frac{1}{\mu_0} \iint_{\Omega_{t2}} (\hat{n}_{t2} \times \mathbf{w}) \cdot \left(\nabla \times \tilde{\mathbf{E}}^i \right) d\Omega \\ &= \iiint_{V_{t1}} \left\{ \frac{1}{\mu_0} (\nabla \times \mathbf{w}) \cdot \left(\nabla \times \tilde{\mathbf{E}}^i \right) + \varepsilon_0\, \mathbf{w} \cdot \frac{\partial^2}{\partial t^2}\tilde{\mathbf{E}}^i \right\} dV \\ &\quad + \iiint_{V_{t2}} \left\{ \frac{1}{\mu_0} (\nabla \times \mathbf{w}) \cdot \left(\nabla \times \tilde{\mathbf{E}}^i \right) + \varepsilon_b\, \mathbf{w} \cdot \frac{\partial^2}{\partial t^2}\tilde{\mathbf{E}}^i + \sigma_b\, \mathbf{w} \cdot \frac{\partial}{\partial t}\tilde{\mathbf{E}}^i \right\} dV. \end{aligned} \quad (11)$$

C. Reflected and Transmitted Fields

As we have mentioned previously, the implementation of the proposed TSFD formulations requires the knowledge of the reflected and transmitted fields from an incident field impinging upon the interface of two homogenous half spaces. In this regard, we follow the frequency-domain technique proposed by [3] for the plane-wave incidence. First, the spectrum of the time-domain incident field is either specified analytically or calculated via FFT from a specified time-domain signal. Then, the spectra of the reflected and transmitted fields are obtained by multiplying the incident field spectrum with the relevant Fresnel reflection and transmission coefficients, respectively. Finally, the time-domain reflected and transmitted fields everywhere in space are calculated via the inverse FFT of the corresponding spectrum after applying an appropriate phase shift. It is worth mentioning that since the dielectric medium is generally treated as lossy or frequency dispersive, the inverse FFT has to be performed at every quadrature point to obtain the desired reflected or transmitted field, and the resultant reflected and transmitted time sequences have to be stored at every quadrature point. However, since the total-/scattered-field boundary is placed very close to any particular scatterer, the excitation region is significantly smaller than the entire computational domain, which significantly mitigates this computational overhead issue. Furthermore, if the medium is lossless, a much simpler procedure is possible since the Fresnel coefficients become frequency independent, and the reflected and transmitted fields can be retrieved by simply applying an appropriate time delay to the incident pulse.

III. Numerical Results

Here, we investigate the accuracy of the proposed TSFD formulations on a cubical volume without a scatterer present. The cubical volume is placed such that its upper half resides in the air region and its lower half in the dielectric region. The dielectric region has a relative permittivity $\varepsilon_{br} = 2.0$ and conductivity $\sigma_b = 0.2$ S/m. The cube that defines the entire computational domain has a side length of 1.0 m, and the first-order ABC is imposed on its surface. The total- and scattered-field interface is defined by another cubical surface with its side length measuring 0.66 m. The incident field is a modulated Gaussian-shaped plane wave polarized parallel to the plane of incidence with an incident angle $\theta = 45^\circ$, with the central frequency $f_0 = 200$ MHz. With no scatterer present in this example, the scatterered field should be ideally zero everywhere inside the computational domain. Therefore, the accuracy of the proposed TSFD formulations can be measured by the root mean square (rms) error in the scattered field in the total- and the scattered-field regions, respectively.

In the simulation, both the total- and the scattered-field regions are discretized with hierarchical higher order tetrahedral elements with a varying order from mixed first to mixed third order. For the temporal discretization, $\Delta t = 5.0 \times 10^{-10}$ s is used, and a total number of 1024 time steps is simulated. Fig. 2 shows the computed rms error at a fixed instant in time in the total- and the scattered-field regions by using the surface formulation and hierarchical vector basis functions of various orders (mixed first, full first, mixed second, full second, and mixed third; see [6] for their detailed description). In both regions, it is found that the rms errors decrease with the increasing mesh density with proper slopes that are dictated by the element order used for discretization. Similar results are obtained for other incident angles (including near-grazing), for the perpendicular polarization, and for the lower half-space with a higher relative permittivity.

However, we found that the volumetric formulation produces rms errors as low as -120 dB in both the total- and the scattered-field regions, independent of the polarization and angle of the incident field, the material property of the dielectric region, and the element size and element order used. It has also been found that this error can be reduced further (to as low as -250 dB as shown in [2]) when a higher precision is used for calculation. This result is well expected by observing the perfect match between the matrices $[\mathbf{T}^t]$, $[\mathbf{B}^t]$, $[\mathbf{S}^t]$ and $[\mathbf{T}^i]$, $[\mathbf{B}^i]$, $[\mathbf{S}^i]$ in (13) in the absence of the scatterer. Therefore, the volumetric formulation is capable of exciting a perfect impressed field in the total-field region with zero leakage into the scattered-field region.

$$
\begin{aligned}
&\iiint_{V_t}\left\{\frac{1}{\mu}(\nabla\times\mathbf{w})\cdot\left(\nabla\times\mathbf{E}^t\right)+\varepsilon\,\mathbf{w}\cdot\frac{\partial^2}{\partial t^2}\mathbf{E}^s+\sigma\,\mathbf{w}\cdot\frac{\partial}{\partial t}\mathbf{E}^t\right\}dV\\
&\quad+\iiint_{V_{s1}}\left\{\frac{1}{\mu_0}(\nabla\times\mathbf{w})\cdot(\nabla\times\mathbf{E}^s)+\varepsilon_0\,\mathbf{w}\cdot\frac{\partial^2}{\partial t^2}\mathbf{E}^s\right\}dV\\
&\quad+\iiint_{V_{s2}}\left\{\frac{1}{\mu_0}(\nabla\times\mathbf{w})\cdot(\nabla\times\mathbf{E}^s)+\varepsilon_b\,\mathbf{w}\cdot\frac{\partial^2}{\partial t^2}\mathbf{E}^s+\sigma_b\,\mathbf{w}\cdot\frac{\partial}{\partial t}\mathbf{E}^s\right\}dV\\
&\quad+Y_0\iint_{\Omega_{s1}}(\hat{n}_{s1}\times\mathbf{w})\cdot\left(\hat{n}_{s1}\times\frac{\partial}{\partial t}\mathbf{E}^s\right)d\Omega+Y_b\iint_{\Omega_{s2}}(\hat{n}_{s2}\times\mathbf{w})\cdot\left(\hat{n}_{s2}\times\frac{\partial}{\partial t}\mathbf{E}^s\right)d\Omega\\
&=\iiint_{V_{t1}}\left\{\frac{1}{\mu_0}(\nabla\times\mathbf{w})\cdot\left(\nabla\times\tilde{\mathbf{E}}^i\right)+\varepsilon_0\,\mathbf{w}\cdot\frac{\partial^2}{\partial t^2}\tilde{\mathbf{E}}^i\right\}dV\\
&\quad+\iiint_{V_{t2}}\left\{\frac{1}{\mu_0}(\nabla\times\mathbf{w})\cdot\left(\nabla\times\tilde{\mathbf{E}}^i\right)+\varepsilon_b\,\mathbf{w}\cdot\frac{\partial^2}{\partial t^2}\tilde{\mathbf{E}}^i+\sigma_b\,\mathbf{w}\cdot\frac{\partial}{\partial t}\tilde{\mathbf{E}}^i\right\}dV
\end{aligned}
\tag{12}
$$

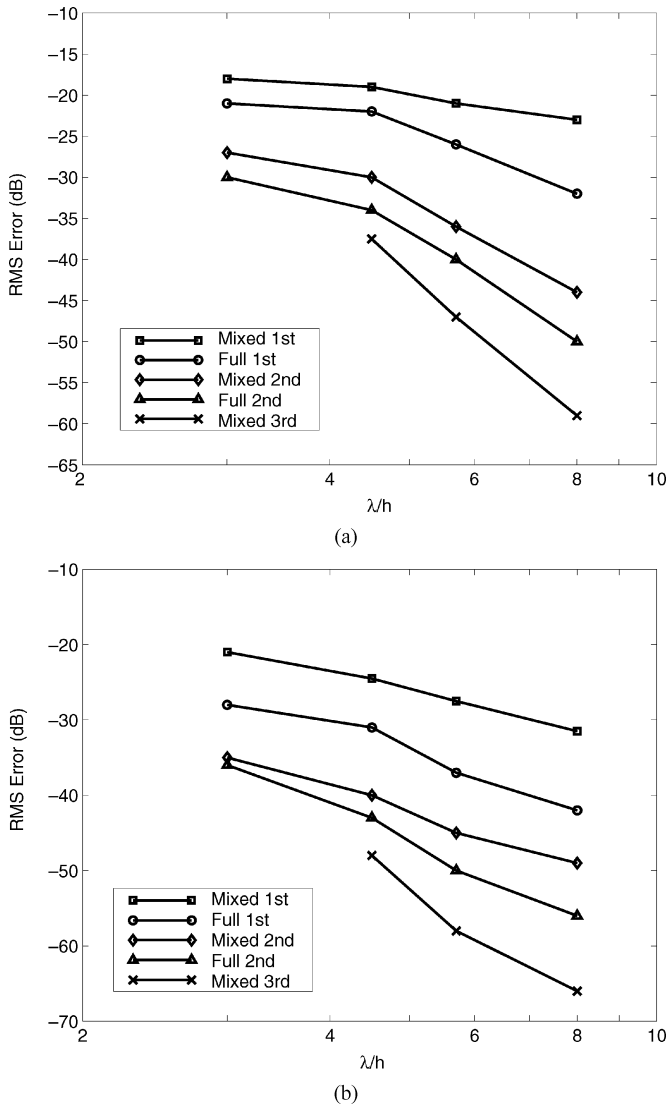

Fig. 2. RMS error in (a) the total-field region and (b) the scattered-field region using the surface formulation, where h is the average element edge length and λ is the free-space wavelength of the central frequency.

We must emphasize that this is the error in the excited field (the field produced by the FETD in the absence of the scatterer), and it is not representative of the accuracy in the final solution when a scatterer is present. Moreover, the implementation of the volumetric formulation requires the calculation of the impressed field over the entire total-field region, whereas the surface formulation requires the impressed field only at the total-/scattered-field interface and inside its neighboring elements. Fig. 3 displays the excited field in the plane of incidence in a computational domain placed across the air–dielectric interface for a horizontally polarized plane wave. To clearly show the wave propagation phenomenon and the transmitted field, we have shifted the central frequency of the modulated Gaussian pulse to 2 GHz, and the conductivity is reduced to $\sigma_b = 0.02$ S/m. In the figure, the horizontal line represents the air–dielectric interface, the larger box represents the entire computational domain, and the smaller box represents the total-field region. The excited field in the scattered-field region, which represents the undesired leakage, is below -120 dB.

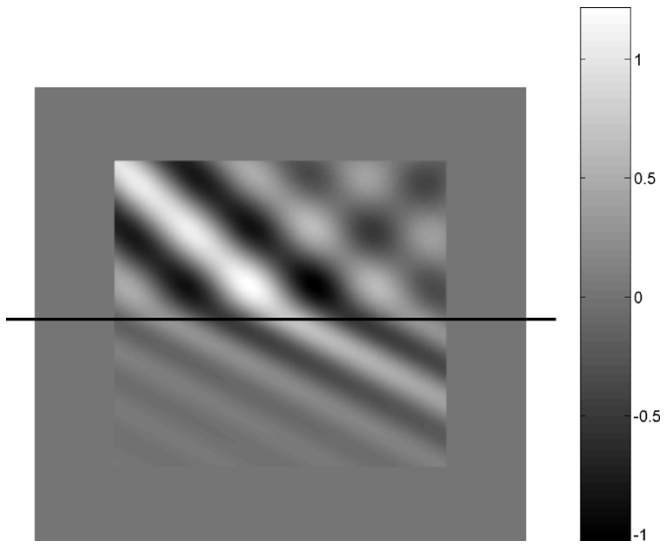

Fig. 3. Snapshot in time of the excited E-field in the total- and scattered-field regions with the computational domain placed across the air-dielectric interface.

IV. Conclusion

The total- and scattered-field decomposition technique, developed earlier for scattering in free space, has been extended for the finite-element time-domain (FETD) modeling of scattering by an object either residing above, partially embedded, or completely buried in a lossy dielectric half-space. Two formulations for exciting the impressed field were described. The volumetric formulation was shown capable of exciting the perfect incident/reflected/transmitted field into the total-field region with zero leakage in the scattered-field region. The surface formulation, closely related to the Huygens' surface concept, was found to excite a less perfect field, with an error associated with the numerical dispersion experienced by the excited field when it propagates from the Huygens' surface through the total-field region. However, such an error can be reduced significantly by the use of higher order basis discretization. The method proposed in this paper can be further extended to the multilayered media in a straightforward manner.

References

[1] J. Jin, *The Finite Element Method in Electromagnetics*, 2nd ed. New York: Wiley, 2002.

[2] D. Riley, J. Jin, Z. Lou, and L. E. R. Petersson, "Total- and scattered-field decomposition technique for the finite-element time-domain method," *IEEE Trans. Antennas Propagat.*, vol. , May 2004, submitted for publication.

[3] K. Demarest, R. Plumb, and Z. Huang, "FDTD modeling of scatterers in stratified media," *IEEE Trans. Antennas Propagat.*, vol. 43, no. 10, pp. 1164–1168, Oct. 1995.

[4] F. L. Teixeira, W. C. Chew, M. Straka, M. L. Oristaglio, and T. Wang, "Finite-difference time-domain simulation of ground penetrating radar on dispersive, inhomogeneous, and conductive soils," *IEEE Trans. Geosci. Remote Sens.*, vol. 36, no. 6, pp. 1928–1937, Nov. 1998.

[5] T. Martin and L. Pettersson, "Modified fresnel coefficients for Huygens' sources in FDTD," *Appl. Comput. Electromagn. Soc. J.*, vol. 17, no. 1, pp. 30–41, Mar. 2002.

[6] J. P. Webb, "Hierarchal vector basis functions of arbitrary order for triangular and tetrahedral finite elements," *IEEE Trans. Antennas Propagat.*, vol. 47, no. 8, pp. 1244–1253, Aug. 1999.

[7] L. E. R. Petersson and J. M. Jin, "An efficient procedure for the projection of a given field onto hierarchical vector basis functions of arbitrary order," *Electromagn.*, vol. 25, no. 2, pp. 81–91, 2005.